2016

Hardware Design and Integration and Software Programming for Optical Elastography

Nima Taherkhani
Michigan Technological University, ntaherkh@mtu.edu

HARDWARE DESIGN AND INTEGRATION AND SOFTWARE PROGRAMMING FOR OPTICAL ELASTOGRAPHY

By

Nima Taherkhani

A THESIS

Submitted in partial fulfillment of the requirements for the degree of

MASTER OF SCIENCE

In Electrical Engineering

MICHIGAN TECHNOLOGICAL UNIVERSITY

2016

This thesis has been approved in partial fulfillment of the requirements for the Degree of MASTER OF SCIENCE in Electrical Engineering.

Department of Electrical and Computer Engineering

Thesis Advisor:	*Dr. Sean Kirkpatrick*
Committee Member:	*Dr. Saeid Nooshabadi*
Committee Member:	*Dr. Smitha Rao*
Department Chair:	*Dr. Daniel Fuhrmann*

Tale of Contents

List of Figures

List of Tables

Acknowledgment

I would like to thank my family for the love and support I've gotten over the years.

I would also like to appreciate Dr. Sean Kirkpatrick for giving me the opportunity to work under his supervision and for his instructions and encouragements through the course of this work.

I wish to express my sincere thanks to Dr. Smitha Rao for the inspirational guidance and help she extended to me whenever I consulted her.

I am also grateful to Prof. Saeed Nooshabadi for accepting to become my committee member.

Finally, I want to take space here to thank Michigan Technological University and the staff and alumni who support this institution, for the opportunities they have created for me throughout my study and into the future.

Abstract

The elastic and viscoelastic properties of skin are a reflection of its health. Measurement of these elastic properties can be used as the indicator of various pathologies. The measurement concept in our works is to mechanically stimulate the skin with a low frequency pneumatic force using non-invasive means of deflecting the skin and use laser speckle to study the elasticity of the skin.

The goal of this work was to develop a setup for in vivo optical elastography of skin. This setup includes an electro-mechanical device which is able to deliver a sinusoidal pneumatic stimulus equivalent to 10 grams of force from a distance of a few centimeters to skin, and a graphical user interface to monitor and control the storage of laser speckle motion on the skin. This thesis describes the hardware design and integrations and software programming of the setup as well as offering an introduction and theoretical overview of optical elastography.

Chapter 1

Introduction

1.1 Elastography; Background and Techniques

It has been well recognized that elastic properties of biological tissue play an important role for diagnosis of pathological change in tissue [1]. The local stiffness of tissue is an indicator of pathological conditions; a locally stiffer region informs about the possible presence of an abnormal growth in the tissue [1]. It is known that detection and characterization of breast tumors can be enhanced by recognizing the difference of elastic modulus among normal soft tissues and malignant tumors [1]. Most cellular diseases change the cellular structure of affected cell, which results in changes of macroscopic mechanical properties of overall tissue [2]. Changes in mechanical properties of tissue provides elastography an opportunity to diagnose and detect the characteristics of the disease [3].

At tissue level, micro-mechanical properties of living tissue depend on the molecular blocks that can reshape the cellular and extracellular structure under mechanical stress [4]. Adhesion force that exists between the layers of

cell are known to regulate the extracellular growth of tissues [5]. The cycled mechanical strain can also be used to regulate the development of engineered smooth muscle tissue [6]. Hence, the pathological changes that occurred in micro-structure of tissue will lead to different biomechanical properties in tissue. Based on different measurement scales, many methods have been used to measure the biomechanical properties to study the tissue health and disease.

Physicians for many years have used palpation to detect pathological change like tumor formation in tissues and qualitatively measure the biomechanical properties of tissues. For quantitavely measuring the biomechanical properties of tissue researchers have developed and utilized biomechanical imaging technologies. Biomechanics is mechanics applied to biology which is described as the study of motion or biological materials and forces that cause such motion [7].

Elastography uses biomedical imaging technologies to study the tissue biomechanical properties. Elastography utilizes the local stiffness in tissue as the contrast mechanism for mapping the elasticity of different region in a tissue.

In this technique, a mechanical force is applied to the tissue by either external or internal stimulation, and simultaneously medical imaging techniques are used to measure the spatial deformation caused by mechanical stimulation, from which elastic modulus can be subsequently estimated.

During the last decades, technologies with capability to generate three-dimensional images have been developed. Computed tomography, magnetic resonance imaging, and ultrasound imaging are three biomedical technologies integrated with elastography technique to measure biomechanical properties in different resolution and penetration scales.

These imaging technologies are categorized based on their penetration depth and resolution scale in table 1-1 and are described in following section.

Table 1-1**:** Different elastography techniques and their features. Data is taken from [3].

Elastographic Imaging Techniques	**Penetration Scale**	**Resolution Scale**
Magnetic Resonance Elastography (MRE)	Entire body	1mm-10mm
Ultrasound Elastography	1mm-10cm	125μm-200μm
Optical Elastography	100μm-3mm	1μm-100μm

Ultrasonic elastography (USE**)** was the first modulus-imaging technology developed for pathological elastography. This technology was developed by Ophir's group at University of Texas Medical School in 1991 [7]. The technique that Ophir's group proposed computes the lap between the pre-compression and post-compression radio frequency ultrasound signals the axial displacement and associated axial strain under quasi-static loading. If a region in tissue has different stiffness than other regions, this technique can distinguish it based on its higher strain level with respect to that of its surrounding regions.

Various methods have been developed for ultrasound elastography. In general, these methods can be categorized into three groups [8]:

First, **static elastography**; in which the displacements of strain resulted from a static compression applied to tissue are measured. During compression and tissue deformation, displacement and time delays between the regions of interest with a few subsequent images are captured [8]. Values for every pixel in elastogram is then calculated from subsequent images. Due to dependence of the applied mechanical force and surrounding tissue, these values are

relative [9]. Therefore, this method of ultrasound elastography is considered as a qualitative technique [8, 9].

Second, **vibro-acoustography** [9], in which the acoustic response of tissue to a harmonic radiation force of ultrasound is used for imaging and material characterization [9]. In this method, two ultrasound beams of slightly different frequencies are focused at the same point, which leads to tissue vibration at a frequency equal to the difference between the frequencies of ultrasound beams. The acoustic response is recorded as the results of raster scanning across the tissue, and then by modulating the amplitude of the acoustic signal from the excitation points, an elastogram of tissue is generated [9]. This method is able to provide quantitative estimations of viscoelastic parameters of biological tissue [8].

Third, **shear wave elastography** and **transient elastography,** which work based on shear waves. Shear wave elastography is based on measuring the velocity of shear wave propagation in soft tissue [9]. In this method an ultrasound probe induces shear waves that propagate from focal point directly in the tissue. A change in the depth of the focal location then leads to interference of shear waves which subsequently results in generation of a

conical shear wave [10]. Shear wave elastography requires fast acquisition of ultrasound images, at least 5000 to 20,000 frames per second for soft tissue [10]. This real-time imaging method can provide 2-dimentional color maps where the color codes quantify the tissue elasticity in terms of kilopascals [9].

Transient elastography functions by inducing a low frequency mechanical force to create a passing distortion in the tissue and using a one-dimensional ultrasound beam to estimate the propagation speed of transient waves, where the propagation speed is slower in soft region than the stiff region of tissue [11]. This method can provide a quantitative data for for tissue elasticity along a line [11].

Magnetic resonance elastography (MRE) is considered as the second generation elastography technology. In this technology, the shear wave (range,50-500 Hz) are induced on surface of tissue using an electro-mechanical transducer and then their propagation is imaged by Magnetic Resonance Imaging (MRI) technique as the imaging modality [12].

In this technology, an additional gradient waveform in the phase-contrast pulse sequence with cyclic motion encoding gradients is synchronized to the mechanical waves in order to sensitize the MRI scan to the propagation wave for imaging the short scale displacements associated with wave propagation.

MRE was first proposed by Ehman et.al (1995) at Mayo Clinic, Plewes, and then was advanced by Sinkus et al. (2000), and Samani et.al (2004) at University of Toronto.

MRE provides deeper imaging in bulk of tissue, so is capable of producing sufficient 3-D spatial and contrast resolution. However, it is significantly more expensive than ultrasound elastography technology.

In addition, the penetration depth of mechanical waves within organic tissue is around a few centimeters. This allows only low-frequency shear waves of about 50-100 Hz be able to penetrate in tissue due to the large frequency-dependent attenuation [12]. This restriction limits the spatial resolution and the achievable detectability of small pathological change when using the MRE.

Optical Elastography is the most recent technique developed for elastographic imaging of tissue. This technique offers higher spatial resolution compared to the previous techniques. In 2-dimentional optical elastography, the stressed tissue is illuminated by a collimated beam and then stiffness is estimated by tracking the motion in the back-scattered speckle pattern resulted from coherently illuminating a stressed object. [13]. Optical elastography offers increased spatial resolution than other elastographic methods. Due to the inherent high-resolution of optical imaging technologies, optical elastography techniques is capable of measuring mechanical properties of tissue at the micron-scale level [14]. Optical elastography is able to provide imaging resolution in range of 1-100 microns, which is the range over which many diseases progress. For example, in diagnosis process of breast cancer, optical elastography is used to evaluate whether cancer has penetrated to basement memberance of an epithelial tumor [15]. Although optical elastography techniques suffer from low penetration depth and can probe only a small area of tissue in one time of test, but because of it fast acquisition speed, high spatial resolution, and large dynamic range of contrast, this technique has been utilized as the handheld probe for tumor margin identification during surgery [16].

Based on different spatial mechanical perturbation characteristics, optical elastography techniques can be classified as internal excitation or external excitation [14], a variety of mechanical excitation have been applied to external optical elastography, including stretch, compression, and wave propagation.

This type of optical elastography was first applied to measure biomechanical properties of *ex vivo* human breast tumor [17]. This system utilizes a low frequency dynamic mechanical waves to drive tissue, and then biomechanical property distribution map of ex vivo human breast are computed by using phase-resolved displacement measurements. Human skin is the other tissue type of interest for biomechanical property measurements using external dynamic optical elastography. This technique works as a tool to study and assess pharmacologic functions of toxins, drugs, and cosmetic treatments. Compared with other technique used for in vivo human skin measurements such as ultrasound imaging, optical elastography techniques can differentiate thicknesses with a resolution in the range of micron and resolve different skin layers and their properties. However, according to implementation characteristics of external excitement methods, external optical elastography

could be impractical for clinical applications in which sterile conditions are required during the measurement, such as measuring biomechanical properties of an exposed tissue surfaces in a surgery [14].

In contrast to external optical elastography technique, in internal elastography techniques, an internal mechanical perturbation is used to stimulate the tissue. An example of this technique is acoustomotive optical coherence elastography reported in [18]. In this technique, an acoustic radiation force is used for internal mechanical excitation and spectral-domain optical coherence tomography (OCT) is used for measuring the mechanical properties.

1.2 Tissue Biomechanics Measurement

Breast and skin are two main objects for the optical imaging techniques. Regarding the breast tumor, optical elastography has been implemented for mammography using optical tomography techniques including both time-domain and frequency-domain methods [20]. Breast tumor development consists of four stages [4]. Stage 1 includes malignant growths which leads the formation of a solid mass. Stage 2 includes the process of tumor formation and growth. Stage 3 includes tumor metastases or cancerous cell spread to

nearby tissue by the bloodstream or the lymphatic circulation. Stage 4 includes metastatic tumor formation at distant locations [4].

Cancer treatments at early stages have the highest chance for success, but are limited to the lack of early-stage detection technologies. While cancerous cell proliferates in the tissue, the microenvironments of tissue supply growth factors to fuel cell proliferation, and promote tumor cell migration through tissue. As tumors grow the microenvironment becomes increasingly turgid because of stromal reorganization. Studies have also revealed that tumor growth is driven by the stiffness of the stromal tissue, primarily by morphogenesis of nearby epithelial cells [8]. Thus, detecting the breast cancer at early stages is critical for either diagnostic and therapeutic purposes. Elastography techniques using optical imaging modalities may provide a solution to quantitatively detect *in vivo* breast tumor development with micron-scale resolution.

Skin is the other study tissue for measurements of biomechanics by optical elastography. Researches on human skin has mainly focus on reconstruction, transplantation, manipulation [21]. Skin maintains many vital complex physiological functions including fluid homeostasis, immune surveillance,

sensory detection, wound healing, and thermoregulation. Skin cells and their layered architecture structure regulate these function. Biomechanical properties of skin are of great importance as they are responsible for skin health and disease, structural integrity, cosmesis, and aging [4]. First studies on skin biomechanics started in the 19th century [22], mainly focusing on skin mechanical anisotropy. Further researches and studies were conducted on skin biomechanical properties in the fields of skin aging [23], sun exposure and skin cancer [24], and cosmetics [25,26].

Various techniques have been developed in literature for measuring skin mechanical properties using optical elastography. Including, a tangential traction method was used to determine the biomechanics of finger pad tissue [27]. Young's modulus, and initial stress of skin also were characterized using a mechanical model under suction [28]. And strain-stress relationships were investigated to study the role of elastin in the mechanical properties of skin [29].

Chapter 2

Theoretical Overview

In this chapter, the focus will be on algorithms and techniques used for measuring and imaging the mechanical properties of skin using optical elastography.

2.1. Elasticity Imaging Methods

As it was discussed earlier, optical elastography is used to quantitatively measure the tissue elasticity. Tissue elasticity imaging methods are based on imaging differences in stiffness or Young's modulus between normal and abnormal skin tissue. **Young's modulus** is defined as the ratio of stress to strain. In biological tissues, the slope of stress-strain curve is called **Young's modulus of elasticity**, or elastic modulus. The steeper the slope, the stiffer the tissue is [30]. Units used to represent it are force per unit area (same as stress) and Pascal (Pas). The Young's modulus is also known as the physical terms corresponding to the parameter used for characterizing the stiffness of

a tissue, which is the quantitative representation of a clinician's palpation and has relevant diagnostic values [30].

To assess the Young's modulus of the tissue, elastography techniques rely on the same basis: an external force is applied to the sample tissue and the resulting movements are then tracked. The external force can be classified according to two means of excitation: the static methods (also called quasi-static method) and the dynamic methods. In static elastography, a constant stress is applied to the tissue and then tissue and the tissue displacement and the generated strain are estimated using image processing techniques. In this method, since the applied stress is unknown, only the strain in tissue can be mapped which is called elastogram.

Although this method has the advantage of being easy to implement but because of unknown stress distribution, static elastography cannot be used for quantitative estimation of the local Young modulus.

In 2-dimentional static optical elastography, tissue displacement in response to mechanical force is measured by speckle tracking.

In dynamic methods, a time-varying mechanical force is applied to the tissue, and then mechanical waves, whose propagation is governed by the tissue

stiffness, is imaged. It can either be a short transient mechanical force or an oscillatory force with a fixed frequency. In this technique, time-varying mechanical perturbations including compressional waves of shear waves are used to stimulate the solid body. This method can produce quantitative and higher resolution Young's modulus map compared to quasi-static methods [30]. However, for using this method use of shear waves a more complex system able to generate the mechanical vibrator or radiation pressure is required.

2.2. Tracking tissue movement

A key part of an elastographic imaging system is the algorithm used to estimate tissue deformation between two frames of optical data. The probe movement in quasi-static elastography is in the axial direction. Hence lateral or elevational tracking, if employed at all, is mainly of use to improve the estimation of the axial deformation [31]. This work is concerned with static speckled-based 2-dimensional optical elastography. In 2-dimensional optical elastography, the movement estimation is based on matching the frames of optical data until some similarity value is optimized. In following, techniques based on speckle shift estimation are introduced.

2.2.1. Laser Speckle Shift estimator

Laser speckle is a physical phenomenon described as the intensity pattern produced by the mutual interference of a set of wavefronts [32]. When the laser light is illuminated on an object, the light waves penetrate to the object and then are scattered by the particles which make up the object. The back-scattered waves that are collected by the photo-detector subsequently generate an interference pattern. This pattern is formed because of the different path lengths that the waves have traveled from object to photo-detector plane. The random phase difference between waves that arrive at photon-detector plane cause constructive and destructive interference, which generate random interference pattern called speckle [33]. Speckle pattern is dependent upon the path difference of the light waves back-scattered from the illuminated object. The displacement occurred in the illuminated area results in speckle pattern fluctuation. The statistic of this fluctuation give information about the displacement and deformation in tissue that causes this to happen.

Due to inhomogeneity of medium in tissue, the light waves penetrate into tissue are subject to rapid decorrelation and depolarization. Two different

estimation schemes insensitive to decorrelation and depolarization of light waves have been proposed for extracting the second order statistic of laser speckle: Parametric and non-parametric shift estimation schemes [34]. Non-parametric schemes include cross-correlation algorithm which calculate the amount of speckle pattern shift by measuring the shift of correlation peak in cross-correlation function of sequential records. In contrast, parametric speckle shift estimator rely on priori assumption of the experiment [34]. An example of this scheme is maximum likelihood shift estimator, which incorporates two assumptions. First the speckle shift is small with respect to the pixel size. Second, the measured laser speckle signal includes a deterministic speckle signal plus noise. In this model, the speckle signal can be shown by [34]:

$$s_j(x_i) = f_j(x_i) + n_j(x_i) \tag{1}$$

where f_j represents the speckle record at j^{th} time sequence, x_i denotes the spatial dimension of pixel i and n_j is a zero-mean noise term at j^{th} time sequence. By calculating the central difference about the j^{th} record, it yields:

$$\begin{aligned} s_{j+1}(x_i+\delta x) - s_{j-1}(x_i-\delta x) = f_{j+1}(x_i+\delta x) - f_{j-1}(x_i-\delta x) \\ + n_{j+1}(x_i+\delta x) - n_{j-1}(x_i-\delta x) \end{aligned} \tag{2}$$

Where δx denotes the shift value in spatial domain. By assuming a constant mean for sequential speckle pattern and Gaussian distribution with zero mean and constant variance, the noise probability density function is given by maximum likelihood [35]:

$$p\left(s_j \mid \mathrm{f}_j\right) = p\left(n_j\right) = C\exp\left\{-\frac{1}{2\sigma^2}\sum_{i=1}^{N}\left[f_{j+1}\left(x_i+\delta x\right)-f_{j-1}\left(x_i-\delta x\right)\right]^2\right\} \quad (3)$$

Where C is a constant. The δx that maximizes the likelihood function can be found by:

$$\frac{\partial}{\partial\left(\delta x\right)}\ln p\left(s_j \mid \mathrm{f}_j\right) = 0 \quad (4)$$

Equation 4 calculates an unbiased estimate of shift in speckle pattern [34].

2.1.2 Imaging system design

Various techniques and systems based on optical elastography have been introduced for elastographic imaging of soft materials and tissues [36, 37, and 38]. In the system proposed by Kirkpatrick and Duncan for mapping the elasticity in vivo human skin lesions with different degree of dermal involvement, a speaker is located 1 cm from the lesion and is driven by a sinusoid signal which generate a Rayleigh wave alongside the lesion. The

lesion and surrounding area are illuminated from an off-axis angle of 40° using a collimated laser beam. Laser speckle motion is then captured by a CCD camera, equipped with an f/2.8 telecentric lens, at a rate of 200 frame/sec from an angle perpendicular to the skin. As pointed by [34], a small amount of misfocus needs to be set to camera lens in order to be able to translate the speckle pattern in space and time, otherwise the intensity visualized by camera would appear to a boiling scene. The magnitude of shift in speckle pattern is visualized as the 2-dimensional shift encoded image using 2-dimensional maximum likelihood shift estimator on a pixel by pixel basis.

Chapter 3

Instrumentation of an electro-optical setup

This chapter discusses design and integration of different parts of the electro-optical setup. In this project, we have developed an electro-mechanical device to deliver a controlled pneumatic stimulus to the surface of skin illuminated by a laser beam, and then capture and save images of resulting speckle motion in a computer for further statistical processing. The experiment is controlled from within a graphical user interface (GUI) programmed in LabVIEW®. A desired stimulation is a sinusoidal pneumatic stimulus with frequency in the range of 1 Hz, which can provide skin deflection by using 10 grams of force at a few centimeters distance. This pneumatic stimulus serves as a non-contact means of deflecting the skin required for non-invasive optical elastography experiment. Mechanical stimulation is incorporated with a collimated laser beam emitter and a CCD camera which are used for generating and capturing laser speckle on skin. Throughout this project, we have created and tested multiple devices that function well individually and then are integrated together to complete the assembly of the setup.

The motivation behind designing this setup was to provide a practical method suitable for elastographic imaging of skin lesions and study and analyze the effects of different moisturizer creams on mechanical properties of skin.

Shown below is a detailed list of a complete setup components and their elements and duties:

- A remotely controllable pneumatic device:
    I. An air flow controller.
    II. An electronic buffer circuit for producing a sinusoidal driving signal as the input of the air flow controller.
    III. A serial connection between buffer circuit and a computer.
- A speckle image recorder :
    I. A CCD camera to record and trigger data at a rate of 200 frame per second.
    II. A f/2.8 lens with 55mm focal length for the speckle and controlling speckle size at the detector plane of CCD camera.

- Graphical user interface:
    I. Control of start and stop of the pneumatic device.

II. Display the camera video output for angle alignment of camera, laser and test sample.

III. Control of the start and stop of the CDD camera recording.

IV. Status bar to indicate recording completion.

- A collimated laser beam emitter for skin illumination.

The hardware integration and software designs of setup are described in following section.

3.1. Hardware Design and Integration

This setup functionally includes three major hardware block which are interfaced with each other using the GUI. The main block in this diagram is a personal computer (PC), which runs the graphical user interface designed for communicating with the CCD cameras and the pneumatic stimulus device. The second block is the CDD camera which is used to record the laser speckle translation. The PC and camera communicate through IEEE-1394b cable as the serial bus which is suitable for high speed communication and real time data transfer. The third block is the buffer circuit which generates the sinusoidal driving signal upon receiving command from PC. This block is

interfaced with PC by USB serial bus and receives data through a USB-TTL converter cable. The fourth block is the pneumatic stimulus device which will produce a sinusoidal puff on the sample. The fifth block in this setup is a green light laser emitter (532 nm). It should be noted that the laser is run independently from rest of the setup. Figure 3-1 shows the hardware blocks diagram of the setup. The initial integration procedures of blocks are described in following section.

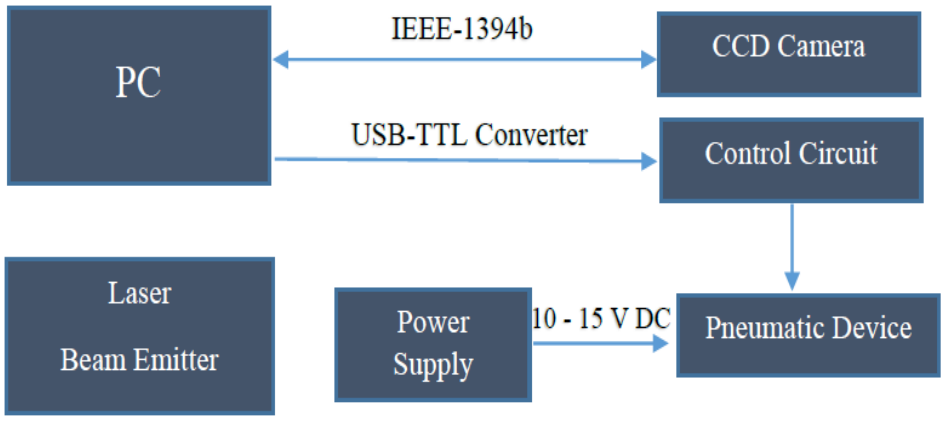

Figure 3-1: Hardware block diagram.

3.1.1. Pneumatic Device

Generating a non-invasive mechanical stimulation is the main concern in the optical elastography experiment. In this work we chose air puff as the

mechanical stimulation the skin due to its safety and feasibility of generation with materials available in the Biomedical Optics lab, where the setup has been assembled. The primary goal is to achieve a sine wave airflow with the frequency of 1 Hz. In this work we used a commercial EVP proportional control valve from Clippard which controls the output air flow based on its input electrical signal. This device has a linear control range with extremely fast reaction time and is capable of producing a smooth sinusoid air flow. The following features are tested in the device test procedure:

- Airflow: Using DC power supply, a function generator and an amplifier circuit sinusoid signals in range of 0.5 to 1.5 Hz are generated, and the output of EVP valve in response to sinusoid signals are measured with a load cell to examine the smoothness of airflow waveform.
- Frequency range: After sinusoidal flow has been established, the achievable range of sinusoidal frequencies in airflow is determined.
- Maximum air pressure: the maximum pressure of airflow at a few centimeters from the proportional valve.

Test results are shown in the table 3.1.

Table 3-1: Pneumatic device test results.

Test	Setup	Result
Airflow	4 V_{pp} 0.5-1.5 Hz sine wave, and amplifier circuit used to generate the driving signal	Acceptable full wave sinusoidal waveform centered at mid-pressure
Frequency range	Load cell to measure air buff pressure	Acceptable response to 0.5-1.5 Hz sine wave signals
Maximum Air Pressure	Load cell to measure air buff pressure	Capable to generate air pressure equivalent to 10 grams in response to 4Volt signal input.

Test results proved that the airflow response is linear and the EVP proportional valve can produce air pressure in the range of 0-15 grams in response to 0-4.2 Volts input signal. This device is presented by Figure 3-2.

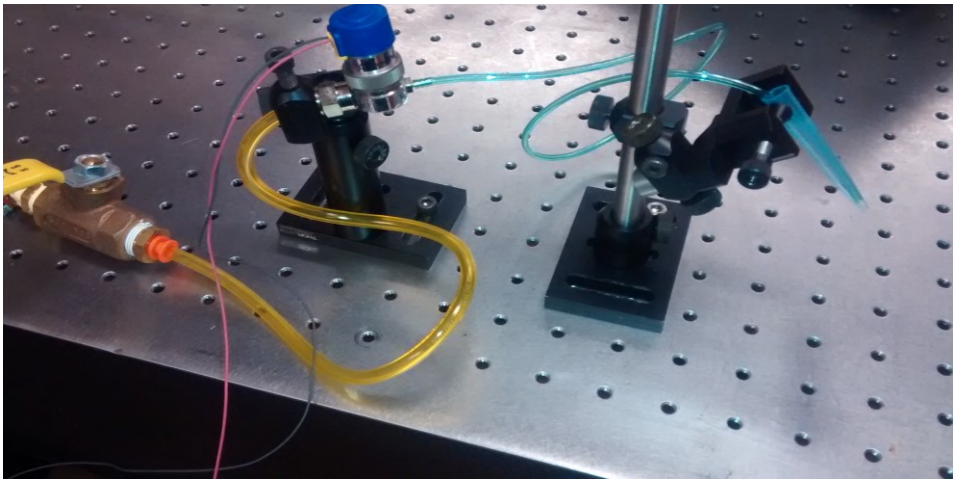

Figure 3-2: The pneumatic device.

3.1.2. Control Circuit

It was proved in pneumatic test procedure that proportional valve performance is dependent on the electronic control circuit. Hence, the requirement for achieving a sinusoidal air puff narrows down to generating a smooth and clean sinusoidal driving signal. This requirement is met by electronic control circuit block. The design of electronic control circuit block includes:

- A switch capable to interface with GUI over USB serial bus.
- A Function generator IC which generates and controls the amplitude and frequency of sinusoidal signal generated for driving the pneumatic device.
- A power amplifier circuit designed for handling the power of the output signal.

Figure 3-3 shows the schematic of the control circuit.

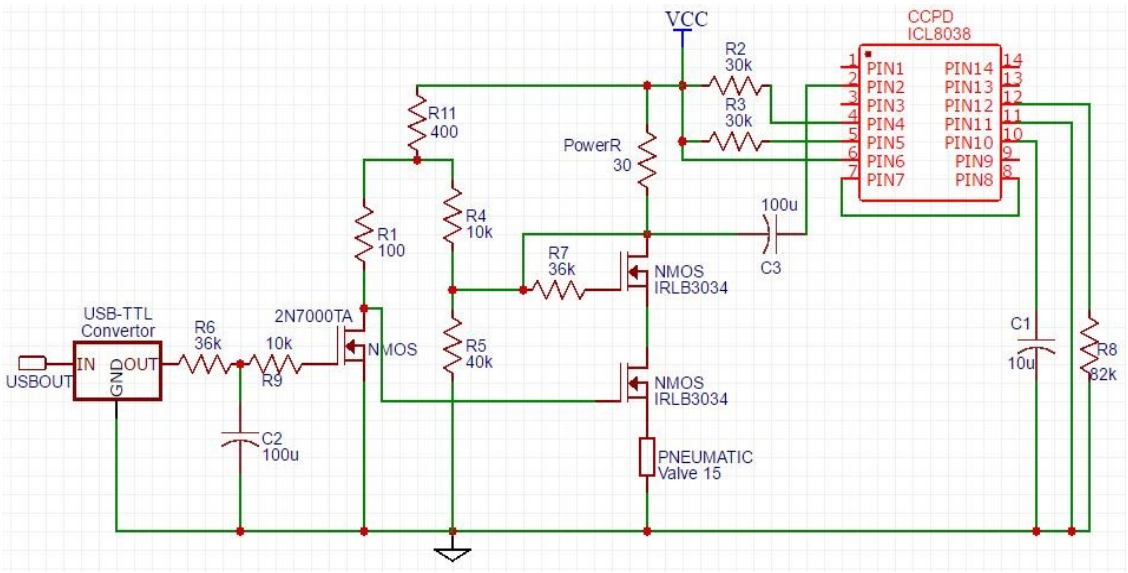

Figure 3-3: Schematic of the control circuit.

The heart of the analog circuit is the ICL 8038 function generator IC which is used for producing sine wave required for generating sinusoidal driving signal. The frequency of output signal is calculated based on the values of resistors and capacitor connected to pin 5, pin 6, and pin 10 respectively. The symmetry of all waveforms can be adjusted with the resistors and capacitor connected to pin 4, pin 5 and pin 10 respectively. R_2 connected to pin 4 and C_1 connected to pin 10 controls the rising time of sine wave. The peak value of sine wave amplitude is set at 1/3 of V_{CC2}. In such a case, the falling time is given by [39]:

$$t_1 = \frac{C_1 \times V_{CC2}}{0.2 \times i_4} = \frac{1/3 \times C_1 \times V_{cc2} \times R_2}{0.2 \times V_{cc2}} = \frac{R_2 \times C_1}{0.6} \quad (1)$$

Where i_4 denotes the input current of pin 4. The falling time of sine wave is controlled by C_1 and R_3:

$$t_2 = \frac{C_1 V_{CC2}}{0.4 i_5 - 0.2 i_4} = \frac{\frac{1}{3} C_1 V_{cc2}}{0.4 \frac{V_{cc2}}{R_3} - 0.2 \frac{V_{cc2}}{R_2}} = \frac{R_2 R_3 C_1}{0.6(2R_2 - R_3)} \quad (2)$$

Where i_5 denotes the input current of pin 5. The frequency of sine wave is given by:

$$f = \frac{1}{t_1 + t_2} = \frac{1}{\frac{R_2 C_1}{0.6}(1 + \frac{R_3}{2R_2 - R_3})} \quad (3)$$

The equal value for rising time and falling time is achieved when $R_2 = R_3 = R$. So then it yields:

$$f = \frac{0.3}{RC_1} \quad (4)$$

By choosing $R_2 = R_2 = 30k\Omega$ and $C_1 = 100\mu f$, we have $f = \frac{0.3}{0.3} = 1\,Hz$.

In order to have the minimum distortion in waveform of IC output signal, pin 7 and pin 8 are short circuited and pin 10 is grounded by an 82 kΩ resistor.

The output signal of IC is fed to the power MOSFET transistors supplied by a variable DC power supply to produce the necessary current to drive the proportional valve.

The connectivity between the PC and control circuit in this design is made through a USB serial bus. A USB-TTL convertor cable is also used to convert the USB output to a logic signal which varies between a high and low level values. Upon receiving high level signal from USB-TTL module, the voltage level in gate of transistor on left side of circuit turns to high which subsequently pulls up the voltage level in the gate side of transistor on right side of circuit presented in Figure 3-3. By triggering the power transistor, the effectual conduit between IC output and proportional valve is formed and the amplified sinusoidal signal is passed to the proportional valve. The analog control circuit allows for real time control over maximum pressure of pneumatic stimulus.

3.1.3. CCD Camera

A CCD camera is used to record the gray-scale changes of the test content. We use a CCD camera manufactured by Point Grey Research which can record images at a maximum of 230 frames per seconds at a resolution of 640×480. Data from camera can be transferred to PC over an IEEE-1394b FireWire connection. Data will be saved to a file location where they can be used then for image processing purposes.

3.2. Software Design

A graphical user interface (GUI) is developed in the National Instrument LabVIEW® programming environment to control each of the hardware block described in the last section. LabVIEW® was chosen as the primary development language because of its flexibility in interfacing with different external devices. It has built-in functions and sessions required to interface with each of communication formats in Figure 3-1. The software block diagram of setup is shown in Figure 3-4.

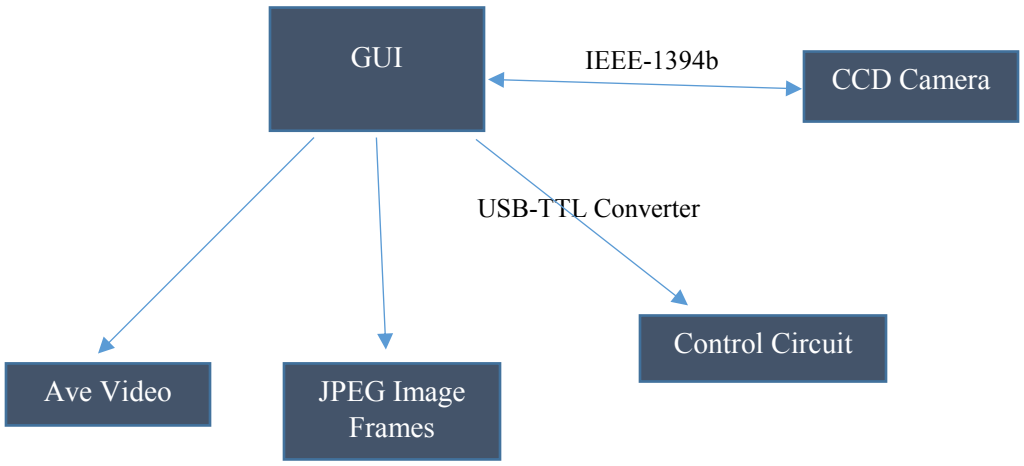

Figure 3-4: Software block diagram.

3.2.1. Camera Software Installation

In order to have the CCD camera operate from the LabVIEW® interface, appropriates software are required to be installed on the PC. Required software as listed below:

- NI LabVIEW
- NI Measurement and Automation Explorer (MAX) software
- NI Vision Acquisition Software with NI-IMAQdx drivers for FireWire camera
- Microsoft Windows 7/8/10.

In order to collect data from camera in LabVIEW, it is important to uninstall the default point grey software drivers previously installed on the PC. Once

the default software is uninstalled, windows will identify the connected camera as the IEEE 1394 host controller. National Instrument's Measurement and Automation Explorer (NI-MAX) and National Instrument's Vision Acquisition interface with NI-IMAQdx driver included are also required to be added to LabVIEW in order to program the camera image acquisition process in the machine.

Once the camera controller driver is configured and NI-MAX and Vision Acquisition Software are installed, the camera setting can be adjusted using the NI-MAX software. By selecting the camera device name that appears in the Devices and Interfaces folder of NI MAX, and opening the camera Attributes tab, the user can adjust the parameters such as auto exposure, brightness, frame rate, gain, shutter speed. Once the desired camera attributes are set, the camera is ready to be integrated with GUI. The complete steps of programming and the camera and control circuit integration with GUI are described in following section.

3.2.2. Programming of GUI

In basic terms, the tasks of GUI are to control the pneumatic device by sending the start and stop command to control circuit and trigger the record operation of desired frame numbers at desired frame rate and then saving the captured laser speckle pattern in a file location.

Shown below is the LabVIEW code developed for realizing the tasks illustrated above. As the Figure 3-5 shows, the code includes two major blocks. Block on the left is responsible for camera initialization and image acquisition process control and block on the right is responsible for interfacing with control circuit. Each block will be described in following section.

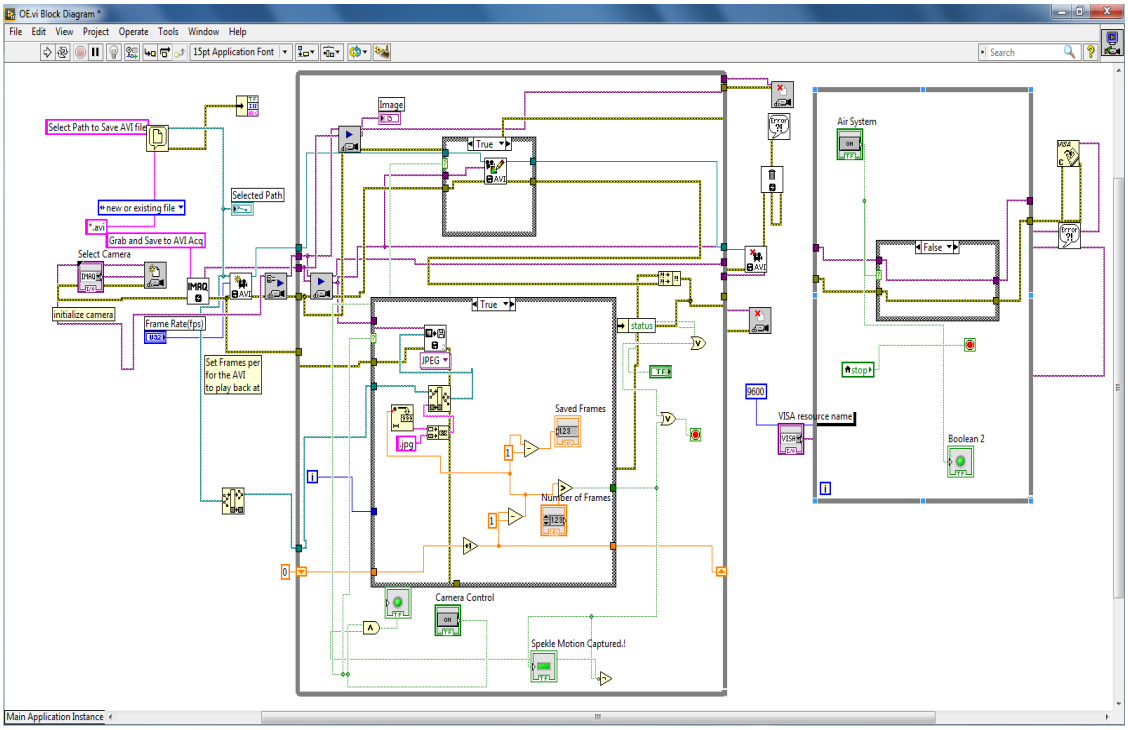

Figure 3-5: Complete code diagram. Screenshot of LabVIEW block diagram. See appendix A for documentation of permission to publish the source code.

- **Image acquisition block: CCD camera initialization and image acquisition**

The individual view of image acquisition block is shown in Figure 3-5. The external while loop of the structure sets up the machine for camera initialization and display the incoming sequence in the display window of the GUI. There are also two case structure inside the while loop. The structure in

bottom waits for a start record button push from user to write the specified number of frames in JPEG format into a pre-allocated location in PC.

Figure 3.5 shows the details of configuration and connections of image acquisition block. The case structure of block is responsible to record the array of images received in the first case structure into an .avi file. This structure runs simultaneously with the first structure on start command from user.

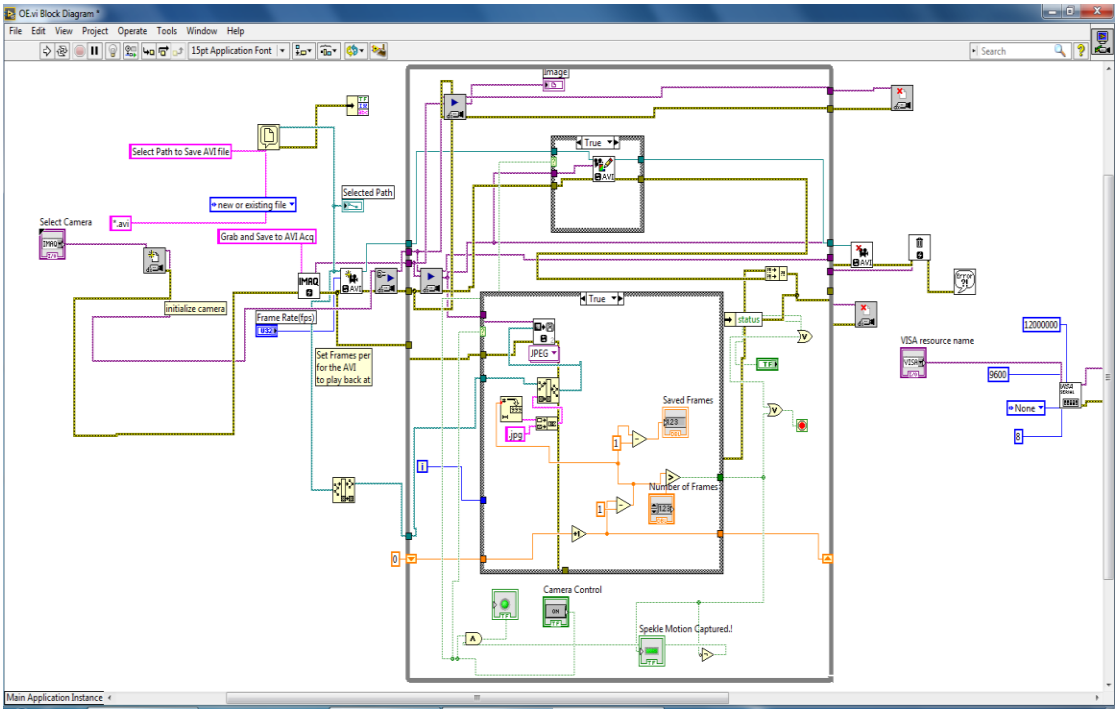

Figure 3-6: Image acquisition block, Screenshot of LabVIEW block diagram. See appendix A for documentation of permission to publish the source code.

- **Serial Interface block: Serial communication with control circuit**

The task of this block is to set up the USB com port for serial communication with the control circuit. In this block, when a start push button is received, the while loop sends binary bits stream over the pre-allocated USB port at a specified baud rate speed. The bit stream transferred by this block is used as the start command in switch part of the control circuit and will trigger the control circuit to generate the driving signal. By terminating the bit stream transmission, the block turns off the driving signal generation. Figure 3-6 shows the detail of serial communication set up and its configuration used in this block.

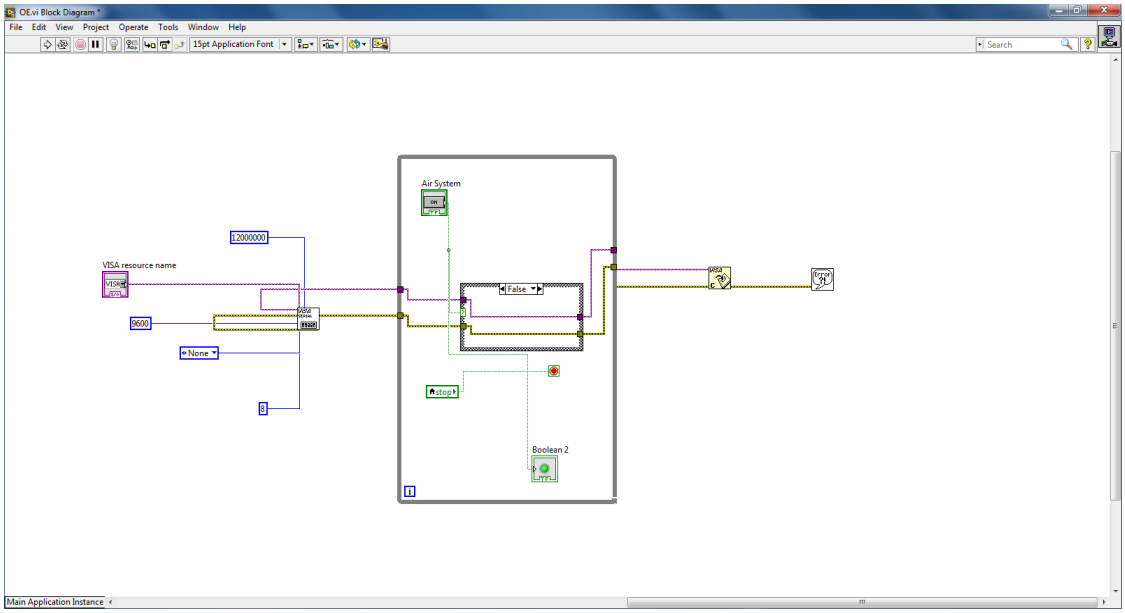

Figure 3-7: Serial communication block, Screenshot of LabVIEW block diagram. See appendix A for documentation of permission to publish the source code.

With these configurations, the programming of GUI is completed.

Chapter 4

Results

After programming the block diagrams, LabVIEW creates the executable VI file of GUI on machine which can be run as a standalone application file. When the GUI file is executed, LabVIEW will first attempt the connection between GUI and the control circuit. If the connection is successful, the LED light installed on the input of circuit will turn on. When the GUI window is open, all features in the camera control section are enabled and camera device selection and USB port allocation can be done in their labeled portals on front panel of GUI as shown in Figure 4-1. The GUI has the ability for the users to specify the number of frames and frame rate of speckle sequence that they wish to capture.

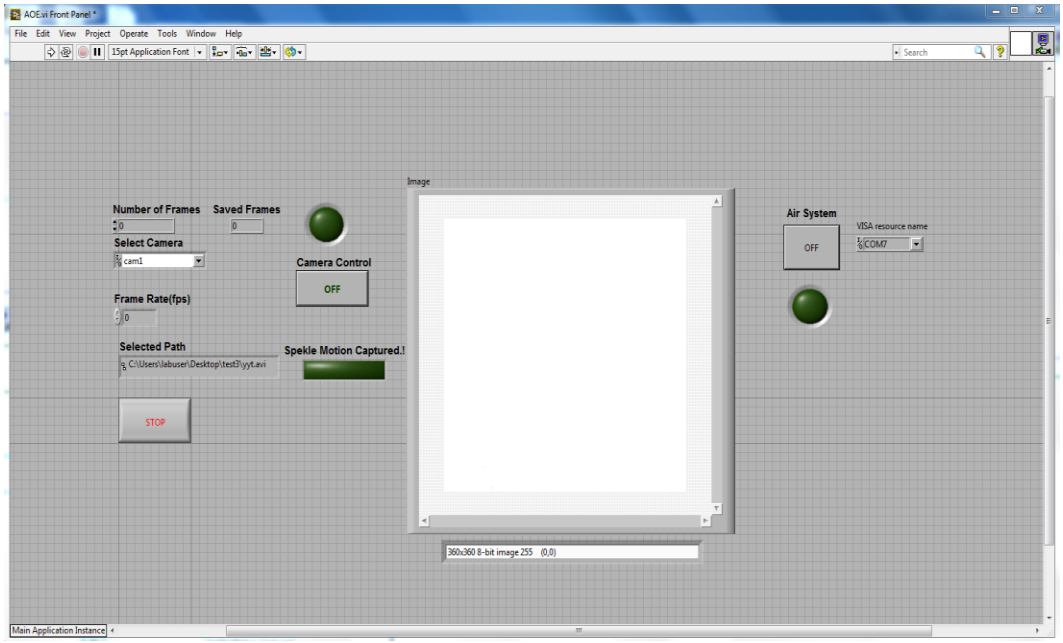

Figure 4-1: GUI when first opened, Screenshot of LabVIEW front panel. See appendix A for documentation of permission to publish the source code.

Once the GUI is run, the image display space will show a live feed of the camera's view as shown in Figure 4-2. User then can save the pre-specified number of frames to the designated folder, given that this folder has been created upon GUI request in very beginning when GUI runs.

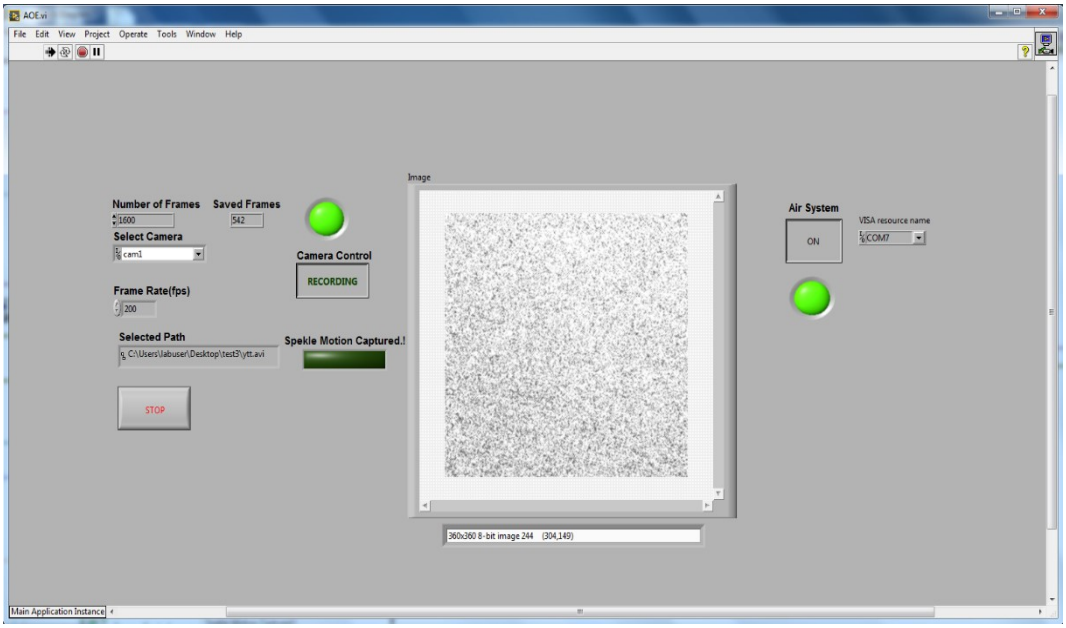

Figure 4-2: GUI after camera initialization, Screenshot of LabVIEW front panel. See appendix A for documentation of permission to publish the source code.

The user is able to control the pneumatic device by using the GUI's air system control button. When the button is pushed, the GUI will start the control circuit to drive the proportional valve and will stop it when the button is switched to off. Below is a step by step instruction on how to use the GUI:

1. Double click on the "Test.vi" file, and open it. This extension has been programmed to certify the user about stable connection between the control circuit and the PC.

I. This LabVIEW extension includes a function code to set up the serial connection between LabVIEW and control circuit through USB port.

II. Run the GUI by clicking on the arrow shape button near the top-left corner of the GUI, and then hit the ON button. Watch the green LED light on the control circuit. When the on button is pressed, the LED light on control circuit loses its brightness. When this is observed, the user can terminate the operation of the GUI by clicking the red circle button near the top-left corner of the GUI and minimize its window.

III. This step guarantees that the serial connection between control circuit and PC is set and the main GUI is ready to work. It should be noted that going through this step is only required in the beginning of operation where the user turns the PC on and wants to run the main GUI for the first time. For next tries of using the main GUI, this step can be skipped.

2. Turn on the DC supply, Open the valve of air pipe, and turn on the red switch on the control circuit. When the switch is on, the red LED on the

control circuit turns to on. When both LED on the control circuit are on, the control circuit is ready to work.

3. The main GUI is labeled as “OE.vi”. Execute it by double clicking on it.
4. Select the camera device in “Select Camera” portal and specify the USB port in “Select USB” portal on front panel of GUI (comm7).
5. Specify the frame rate in “Frame Rate” portal.
6. Specify the number of frames that you want to capture from speckle motion.
7. Run the GUI.
    I. A windows will be popped up at beginning which request for a path to save images and video sequence. Select or generate a folder and then specify a name for video sequence and click the OK button on window to close it.
    II. Click the button labeled as “Air System” control to run the mechanical stimulation system.
    III. Once the camera settlement and angle is set and ready for the experiment, hit the button labeled as” Camera Control”.
    IV. When the all frames designated in section 5 are buffered and saved, frame capturing process will be terminated automatically

and LED labeled as “Speckle Motion Captured” in GUI will notify user of that. At this moment user can terminate the GUI.

Going through step 1 is recommended to make sure that USB device stay identified in PC during the GUI operation.

To test the functionality of control circuit, a load cell with proportional output is connected to the pneumatic device and the output voltage is connected to an oscilloscope to verify that the waveform of airflow appears sinusoidal. Figure 4-3 shows the signal output of load cell when pneumatic device is running. Figure 4-4 shows the skin deformation generated by pneumatic device.

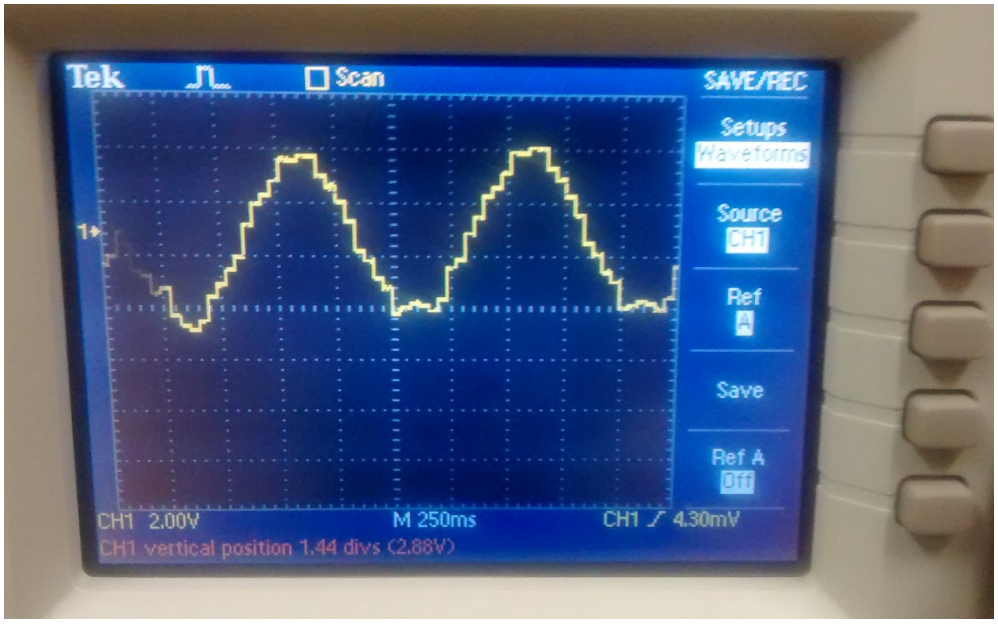

Figure 4-3: Signal waveform of a load cell located 0.5 cm from the proportional valve.

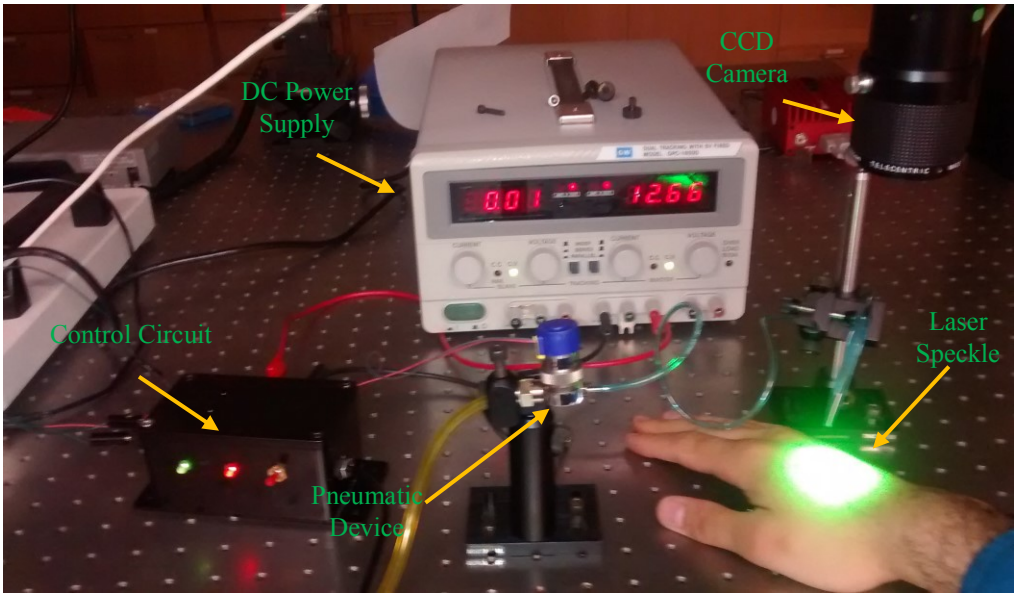

(a)

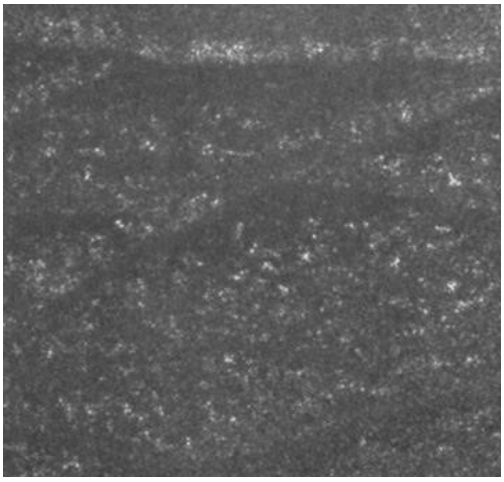

(b)

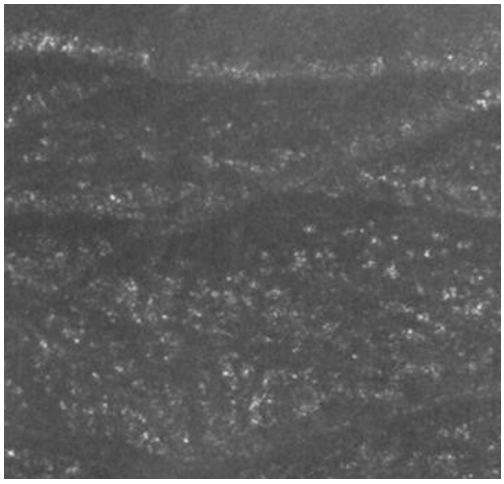

(c)

Figure 4-4: Optical elastography of hand skin. a) Laboratory set-up for in vivo optical elastography. b) Hand skin before deformation. c) Hand skin after deformation.

Chapter 5

Conclusions and Future Work

5.1. Summary and Conclusion

The objective of this work was to develop a setup for optical elastography of skin. All major tasks of the project where accomplished which includes designing an analog buffer circuit that drives a proportional valve to apply a sinusoidal pneumatic stimulus with frequency in the range of 1 Hz and maximum mechanical force in range of 10 g to the test sample located at a few centimeter from the valve, and programming a LabVIEW GUI which provides the ability to start and stop the pneumatic stimulus applied to the skin, and display and control the storage of data from a CCD camera.

While there are some improvements that can be made to promote the setup in the future, it can work well for one-dimensional elastographic imaging experiments.

5.2. Suggestion for Future Work

The setup developed here can be improved should additional features are added:

- A secondary microcontroller can be programmed and integrated to control circuit to vary the resistors connected to pin 4 and pin 5 of the function generator IC based on the command received from GUI and in this way it can change the frequency of driving signal delivered to pneumatic device. This feature would be helpful for experiments that require stimulating the sample test by mechanical forces with different frequencies.

- The MATLAB code written for generating elastogram can be compiled to create an executable file. This file can then be called in GUI to process the data received from camera and display the processing result and the elastogram calculated by MATLAB code.

- # References

1- Satyanand Tyagi, Sachin Kumar. "*Clinical Applications of Elastography: An Overview*," International Journal of Pharma and Bio Sciences, 2010.

2- Andrea Curatolo, Martin Villiger, Dirk Lorenser, Philip Wijesinghe, Alexander Fritz, Brendan F. Kennedy, and David D. Sampson, "*Ultrahigh-resolution optical coherence elastography*," Opt. Lett. 41, 21-24 (2016)

3- Ophir, J et al. J Med Ultrasonics (2002) 29: 155. doi:10.1007/BF02480847.

4- Xing Liang. (2010). "*Coherence Imaging Technologies for the Measurement of Tissue and Cell Biomechanics*," (Doctoral Dissertation). Retrieved from : https://www.ideals.illinois.edu/bitstream/handle/2142/16859/1_Liang_Xing.pdf?sequence=3

5-B. I. Shraiman, "*Mechanical feedback as a possible regulator of tissue growth*," Proceedings of the National Academy of Sciences of the United States of America, vol. 102, pp. 3318-3323, March 1, 2005.

6-B. S. Kim, J. Nikolovski, J. Bonadio, and D. J. Mooney, "*Cyclic mechanical strain regulates the development of engineered smooth muscle tissue*," Nat Biotechnol, vol. 17, pp. 979-83, Oct 1999.

7- Ophir et al., 1991 & 1999; Garra et al., 1997; Righetti et al., 2002

8- - Zaleska-Dorobisz, U., Kaczorowski, K., Pawluś, A., Puchalska, A. & Inglot, M. "*Ultrasound elastography-review of techniques and its*

clinical applications," Adv Clin Exp Med. **23,** 645–655 (2014).

9- Bamber J**, "***EFSUMB guidelines and recommendations on the clinical use of ultrasound elastography. Part 1: Basic principles and technology*," Ultraschall Med 2013 Apr, 34, 169–184.

10-S. Castéra L, Vergniol J, Foucher J, Le Bail B, Chanteloup E, Haaser M, de Lédinghen **V, "***Prospective comparison of transient elastography, Fibrotest, APRI, and liver biopsy for the assessment of fibrosis in chronic hepatitis C*," Gastroenterology 2005, 128, 343–350.

11- - Kirk GD, Astemborski J, Mehta SH, Spoler C, Fisher C, Allen D, Higgins Y, Moore RD, Afdhal N, Torbenson M, Sulkowski M, Thomas DL**, "** *Assessment of Liver Fibrosis by Transient Elastography in Persons with Hepatitis C Virus Infection or HIV–Hepatitis C Virus Coinfection*," Clin Inf Dis 2009, 48, 963–972.

12- Venkatesh SK, Yin M, Ehman RL (2013) "*Magnetic resonance elastography of liver: technique, analysis, and clinical applications*," J Magn Res Imaging 37:544–555

13- Donald D. Duncan; Sean J. Kirkpatrick; "*Processing techniques for laser speckle derived from biological tissues*," Proc. SPIE 3914, Laser-Tissue Interaction XI: Photochemical, Photothermal, and Photomechanical, 639 (June 13, 2000); doi:10.1117/12.388088.

14- Xing Liang CRECEA V, BOPPART SA. *Dynamic Optical Coherence Elastography: A Review,"* Journal of innovative optical health sciences. 2010; 3(4):221-233. Doi: 10.1142/S1793545810001180.

15- David Sampson "*Optical elastography Prospects in medicine for micro-imaging of tissue mechanical properties*," School of Electrical, Electronic and Computer Engineering, The University of Western Australia. Retrieved from:

https://www.asp.uni-jena.de/aspmedia/Downloads_guest_professors/David+D+Sampson/Sampson+Lecture+4+Elastography.pdf

16- Luo W, Nguyen FT, Zysk AM, Ralston TS, Brockenbrough J, Marks DL, Oldenburg AL, Boppart SA. "*Optical biopsy of lymph node morphology using optical coherence tomography*," Technology in Cancer Research & Treatment, 4:539-547, 2005.

17- Xing Liang, Amy L. Oldenburg, Vasilica Crecea, Eric J. Chaney, and Stephen A. Boppart, "*Optical micro-scale mapping of dynamic biomechanical tissue properties*," Opt. Express 16, 11052-11065 (2008).

18- Xing Liang, Orescanin M, Toohey KS, Insana MF, Boppart SA. "*Acoustomotive optical coherence elastography for measuring material mechanical properties*," Optics letters. 2009; 34(19):2894-2896.

19- V. Spinelli L, Torricelli A, Pifferi A, Taroni P, Danesini G, and Cubeddu R. " *Characterization of female breast lesions from multi-wavelength time-resolved optical mammography*," Phys Med Biol 50 (11), 2489–2502, 2005.

20-L. C. Enfield, A. P. Gibson, J. C. Hebden, and M. Douek, "*Optical tomography of breast cancer-monitoring response to primary medical therapy*," Targeted Oncology, vol. 4, pp. 219-233, Sep 2009

21- D. A. Medalie, S. A. Eming, M. E. Collins, R. G. Tompkins, M. L. Yarmush, and J. R. Morgan, "*Differences in dermal analogs influence subsequent pigmentation, epidermal differentiation, basement membrane, and rete ridge formation of transplanted composite skin grafts*," Transplantation, vol. 64, pp. 454-65, Aug 15 1997.

22- B. J. Wilhelmi, S. J. Blackwell, and L. G. Phillips, "*Langer's lines: To use or not to use,*" Plastic and Reconstructive Surgery, vol. 104, pp. 208-214, 1999.

23- H. G. Vogel, "*Directional variations of mechanical parameters in rat skin depending on maturation and age*," J Invest Dermatol, vol. 76, pp. 493-7, Jun 1981.
24- Y. Nishimori, C. Edwards, A. Pearse, K. Matsumoto, M. Kawai, and R. Marks, "*Degenerative alterations of dermal collagen fiber bundles in photodamaged human skin and UV-irradiated hairless mouse skin: possible effect on decreasing skin mechanical properties and appearance of wrinkles*," J Invest Dermatol, vol. 117, pp. 1458-63, Dec 2001.

25- Han-Jo Ko, Wei Tan, Ron Stack, and Stephen A. Boppart. "*Optical Coherence Elastography of Engineered and Developing Tissue*," Tissue Engineering. February 2006, 12(1): 63-73. doi:10.1089/ten.2006.12.63.

26- D. C. Salter, H. C. McArthur, J. E. Crosse, and A. D. Dickens, "*Skin mechanics measuredin vivo using torsion: a new and accurate model more sensitive to age, sex and moisturizing treatment*," Int J Cosmet Sci, vol. 15, pp. 200-18, Oct 1993.

27- Q. Wang and V. Hayward, "*In vivo biomechanics of the fingerpad skin under local tangential traction*," J Biomech, vol. 40, pp. 851-60, 2007.

28- S. Diridollou, D. Black, J. M. Lagarde, Y. Gall, M. Berson, V. Vabre, F. Patat, and L. Vaillant, "*Sex- and site-dependent variations in the thickness and mechanical properties of human skin in vivo*," Int J Cosmet Sci, vol. 22, pp. 421-435, Dec 2000.

29- H. Oxlund, J. Manschot, and A. Viidik, "*The role of elastin in the mechanical properties of skin,*" J Biomech, vol. 21, pp. 213-8, 1988.

30-J.-L. Gennisson, T. Deffieux, M. Fink, M. Tanter " *Élastographie ultrasonore : principes et procédés Journal de Radiologie Diagnostique et Interventionnelle,"* Volume 94, Issue 5, May 2013, Pages 504-513

31- Graham Treece, Joel Lindop, Lujie Chen, James Housden, Richard Prager, Andrew Gee Interface Focus 2011 -; DOI: 10.1098/rsfs.2011.0011. Published 20 April 2011.

32- Karan D. Mohan and Amy L. Oldenburg, "*Elastography of soft materials and tissues by holographic imaging of surface acoustic waves*," Opt. Express 20, 18887-18897 (2012).

33- Boas DA, Dunn AK. "*Laser speckle contrast imaging in biomedical optics*," Journal of Biomedical Optics. 2010;15(1):011109. doi:10.1117/1.3285504.

34- Donald D. Duncan, Sean J. Kirkpatrick; "*Maximum-likelihood estimators for one- and two-dimensional speckle motion*," Proc. SPIE 4961, LaserTissue Interaction XIV, 202 (July 23, 2003); doi:10.1117/12.477914.

35- - B. R. Frieden. "*Probability, Statistical Optics, and Data Testing: A Problem Solving Approach*," Second Edition, Springer-Verlag, Berlin (1991).

36- Sean J. Kirkpatrick, Ruikang K. Wang, Donald D. Duncan, Molly KuleszMartin, and Ken Lee, *"Imaging the mechanical stiffness of skin lesions by in vivo acousto-optical elastography*," Opt. Express 14, 9770-9779 (2006).

37- Qi W, Chen R, Chou L, et al; "*Phase-resolved acoustic radiation force optical coherence elastography*," J. Biomed. Opt. 0001; 17(11):110505-110505. doi: 10.1117/1.JBO.17.11.110505.

38- Chunhui Li, Guangying Guan, Xi Cheng, Zhihong Huang, and Ruikang K. Wang, "*Quantitative elastography provided by surface acoustic waves measured by phase-sensitive optical coherence tomography*," Opt. Lett. 37, 722-724 (2012).

39- Intersil® (April 2001). "*ICL8038, Precision Waveform Generator/Voltage Controlled Oscillator*," [Online]. Available:

www.intersil.com/content/dam/Intersil/documents/icl8/icl8038.pdf [June 25, 2016

Appendix A

Permission to Publish LabVIEW GUI Source Code

The permission to publish the LabVIEW GUI source codes in Figure 3-5, Figure 3-6, Figure 3-7, Figure 4-1, and Figure 4-2 is provided by the following addendum of National Instrument software license agreement:

National Instrument Software License Agreement

ADDENDUM A – Source Code License:

1. "Source Code" means the NI-created human-readable computer code that NI provides with the Software, that is not password protected, and that is in the preferred form for modifying the code (whether graphical or text-based). Source Code does not include any Third Party Software.
2. This license permits you to use, modify, and distribute the Source Code on the conditions that
   A. you may distribute the Source Code, whether or not you have modified it, only
      I. for a non-commercial purpose and

II. under a license identical to this Source Code License;

B. you may distribute object code derived from the Source Code, whether or not you have modified it, for any purpose;

C. you maintain and do not minimize, block, or modify any titles, logos, trademarks, copyright, digital watermarks, disclaimers, or other notices that are included in the Source Code;

D. You agree that the copyright holders(I) provide the software "as is" with all fault (known and unknown) and without any warranty, representation, or other guarantee of any kind and (II) disclaim all warranties, representations, and other guarantees relating to your use, modification, or distribution of the source code, whether express, implied, or statutory, including any warranty of title, implied warranty of merchantability, fitness for a particular purpose, and non-infringement, and any implied warranty arising out of course of dealing performance or trade usage.

E. You assume all of the risk and liability associated with your use, modification, or distribution of the source code;

F. You agree that the copyright holders are not liable to you for, and you agree not to assert any claim against any copyright holder or its directors, officers, employees, or agents for, any damage, loss, or other prejudice

of any kind, however caused, and on any theory of liability, or tort(including negligence), that arises in any way out of the use, modification, or distribution of the source coded, even if the copyright holder was advised of the possibility of any such damage, loss, or other prejudice, including any damage, loss, or other prejudice that (I) is lost profits (weather yours or personal) or intangible property (including software and data); Arises out of or relates to any temporary or permanent loss of tangible property (weather real or personal) or (III) is direct, special, indirect, incidental, consequential, collateral, exemplary, punitive, or any other damage; and,

G. you agree that these Sections 1-3 express the entire agreement between you and the copyright holders regarding your use, modification, and distribution of the Source Code.

3. The copyright holders reserve all of their rights. Except for the non-exclusive licenses expressly granted in Section 2, no rights or licenses are granted expressly, by implication, or otherwise.